The Effects of Structural and Microenvironmental Disorder on the Electronic Properties of Poly[2-methoxy,5-(2′-ethyl-hexoxy)-1,4-phenylene vinylene] (MEH−PPV) and Related Oligomers

Sebastian Wachsmann-Hogiu,† Linda A. Peteanu,* Limin Angela Liu, and David J. Yaron*

Department of Chemistry, Carnegie Mellon University, Pittsburgh, Pennsylvania 15213

Jurjen Wildeman

Department of Polymer Chemistry and Materials Science Centre, University of Groningen, Nijenborgh 4, 9747 AG Groningen, The Netherlands

Received: October 22, 2002; In Final Form: April 1, 2003

In this study, electroabsorption (Stark) spectroscopy is used to determine the trace of the change in polarizability (tr $\overleftrightarrow{\Delta\alpha}$) and the absolute value of the change in dipole moment ($|\Delta\vec{\mu}|$) of the electroluminescent polymer poly[2-methoxy,5-(2′-ethyl-hexoxy)-1,4-phenylene vinylene] (MEH−PPV) and several model oligomers in solvent glass matrixes. We find a value of tr $\overleftrightarrow{\Delta\alpha}$ of ∼2000 Å^3 for the polymer and for a 9-ring substituted oligomer in both toluene and 2-methyl tetrahydrofuran matrixes at 77 K with smaller values being obtained for 3- and 5-ring unsubstituted oligomers. Although gas-phase calculations of tr $\overleftrightarrow{\Delta\alpha}$ using INDO/SCI yield values that are about a factor of 8 smaller than the experiment, excellent agreement is obtained when the effects of solid-state dielectric screening are included. Screening increases tr $\overleftrightarrow{\Delta\alpha}$ by bringing the energy gap between the $1B_u$ and mA_g states into agreement with solid-state measurements. Substantial values of $|\Delta\vec{\mu}|$ are observed experimentally both for the polymer and for the oligomers (6−11 D). Because in a planar (C_{2h}) geometry the oligomer and polymer are centrosymmetric, the observed $|\Delta\vec{\mu}|$ is an indication of disorder-induced symmetry breaking in the material. Calculations indicate that disorder in the ground-state geometry of the polymer (inner-sphere disorder) can account for nearly half of the observed $|\Delta\vec{\mu}|$. Disorder in the glassy environment (outer-sphere disorder) leads to a nonuniform electrostatic environment, and calculations show that this is a substantial contributor, accounting for the remainder of the observed $|\Delta\vec{\mu}|$.

Introduction

Because of their favorable fluorescence properties, poly(*p*-phenylene vinylene) (PPV) and its derivatives such as poly[2-methoxy,5-(2′-ethyl-hexoxy)-1,4-phenylene vinylene] (MEH−PPV) (Scheme 1) and others are well suited for photophysical applications such as light-emitting diodes,[1,2] lasers,[3−6] and analyte detectors.[7] To optimize these materials for applications, a number of important photophysical issues must be addressed. These include determining how chain length, conformation, and the properties of the matrix containing the polymer affect the delocalization length of the excitation on the polymer (size of the exciton). Likewise, the complex interplay between film morphology, molecular conformation, and photophysics is of substantial current interest.[8−16] One specific goal of understanding this relationship is the ability to use the optical and electronic properties of these materials as a qualitative and perhaps quantitative gauge of the extent of disorder or aggregation or both in the sample. Disorder and aggregation are important because of their profound effect on the luminescence yield and charge transport efficiencies of MEH−PPV and related molecules and therefore on the overall efficiency of LED devices fabricated from them.

Electroabsorption is a technique that permits the measurement of two fundamental electronic properties of a molecule, namely, the trace of the change in polarizability, tr $\overleftrightarrow{\Delta\alpha}$, and the absolute change in dipole moment, $|\Delta\vec{\mu}|$, on excitation by analysis of the shift in the absorption band of a frozen isotropic sample in an applied electric field. The value of tr $\overleftrightarrow{\Delta\alpha}$ is frequently associated with the size of the exciton in a given material, a quantity that is often related to charge mobility through the molecular skeleton.[17,18] The quantity $|\Delta\vec{\mu}|$ is associated with the charge-transfer character of the optical transition. For symmetric molecules, $|\Delta\vec{\mu}|$ is expected to be zero, though disorder can break the symmetry of the molecule and allow a substantial $|\Delta\vec{\mu}|$ to be observed.

Previously, we have applied this technique to films of emeraldine base (EB) and of a 5-ring model oligomer dispersed in a poly(methyl methacrylate) (PMMA) matrix.[19] These measurements revealed a surprisingly large $|\Delta\vec{\mu}|$ in this nominally symmetric molecule. Using electronic structure calculations to probe the source of the symmetry breaking, we found that small torsions of the rings of the molecule were sufficient to induce net charge-transfer character in the optical absorption band. In this system, the experimentally measured $|\Delta\vec{\mu}|$ could be rationalized solely on the basis of this intramolecular structural disorder without the need to invoke additional disorder arising from the glassy matrix. Because the value of tr $\overleftrightarrow{\Delta\alpha}$ of EB is relatively small (200 ± 20 Å^3), one would *not* expect a significant contribution from induced moments due to local fields.

Here, we apply the same technique to measure the electronic properties of MEH−PPV and several model oligomers (Scheme 1) dispersed in solvent glass matrixes, focusing on the transition

* To whom correspondence should be addressed. E-mail addresses: yaron@cmu.edu; peteanu@andrew.cmu.edu.

† Present address: Cedars-Sinai Medical Center, Los Angeles, CA 90048.

10.1021/jp0272769 CCC: $25.00
Published on Web 05/10/2003

SCHEME 1[a]

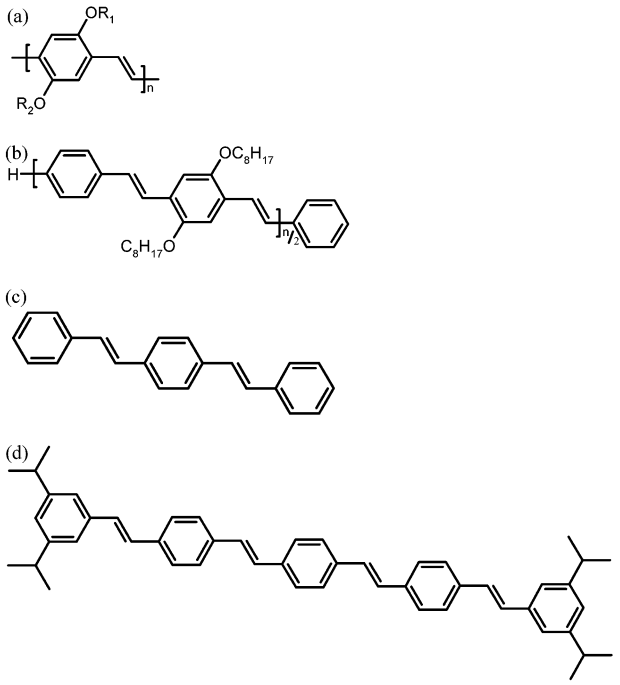

[a] (a) The repeat unit of MEH−PPV. R_1 = methyl; R_2 = 2-ethylhexyl; $n \gg 100$. (b) The oligomer OPPV-9. (c) PPV-3. (d) PPV-5.

between the ground ($1A_g$) and the lowest excited ($1B_u$) electronic states. Once again, the observed $|\Delta\vec{\mu}|$'s are found to be fairly large ($|\Delta\vec{\mu}| > 6$ D), though the molecules are nominally symmetric. However, unlike EB, these molecules all exhibit significant tr $\overleftrightarrow{\Delta\alpha}$'s, making them potentially more sensitive probes of local fields in their environment. The observed values of tr $\overleftrightarrow{\Delta\alpha}$ are, in fact, a factor of 8 larger than what would be predicted based on INDO/SCI finite field calculations of the *gas-phase* polarizabilities of a planar oligomer. However, when the electronic states of this molecule are solvated, using the methodology of Moore et al.,[20] good agreement between experimental and calculated polarizabilities is obtained. Cast in the language of continuum solvation theory, the method accounts for the enhancement of tr $\overleftrightarrow{\Delta\alpha}$ due to the reaction field arising from the high-frequency dielectric response of a nonpolar environment. The high-frequency dielectric response screens the electron−hole interaction in the excited states, lowering the energy gaps between the excited states and increasing their polarizability. Of particular importance is the energy gap between the $1B_u$ and mA_g state. The mA_g state carries most of the optical intensity out of the $1B_u$ state,[21] and electron−hole screening must be included to obtain calculated values for the $1B_u-mA_g$ energy gap that are in agreement with experiment. Properly accounting for this electron−hole screening effect also proved critical to successfully modeling the origin of the experimental $|\Delta\vec{\mu}|$, as will be shown below.

The observation of a nonzero $|\Delta\vec{\mu}|$ in nominally symmetric (C_{2h}) polyenes has ample precedent in the literature. Values of $|\Delta\vec{\mu}|$ of up to 20 D have been measured for carotenoids entrained in protein matrixes, which have been attributed to substantial organized fields in these environments.[22,23] Typically, polyenes and smaller carotenoids have exhibited $|\Delta\vec{\mu}|$'s of 1−5 D even in polymer and solvent glass matrixes.[24−27] Likewise, a $|\Delta\vec{\mu}|$ of 50 D was reported for the highly polarizable polymer polydiacetylene.[28]

One of the most detailed studies of this phenomenon in polyenes was performed by Kohler and co-workers, who observed splittings in the narrow holes burned in the $2A_g-1A_g$ transition of octatetraene entrained in a polycrystalline *n*-alkane matrix at 1.7 K.[29,30] The line shape of this high-resolution Stark spectrum was successfully modeled by taking into account the orientations of the alkane molecules surrounding the octatetraene probe, as well as their detailed charge distributions. From this it was concluded that the local fields due to the C−H bonds of the alkanes create substantial internal fields that add vectorially to the externally applied field acting on the octatetraene and lead to splitting of the hole.

These studies all suggest that internal fields in the environment can induce dipoles in a polarizable molecule that are manifested as a bulk $|\Delta\vec{\mu}|$ in an electroabsorption experiment. Here, to mimic this disorder due to the local environment (outer-sphere disorder), we surround a planar symmetric model oligomer of PPV either with explicit solvent molecules or with a matrix consisting of random dipoles. We find that a substantial $|\Delta\vec{\mu}|$ can be induced in this fashion, but *only* if the electron−hole screening arising from the fast dielectric response of the environment is also included.

Motivated by the success of our earlier studies on EB,[19] we also examined the effect of twisting about the single bonds of a model oligomer of PPV (inner-sphere or geometric disorder) on both tr $\overleftrightarrow{\Delta\alpha}$ and $|\Delta\vec{\mu}|$ of the molecule. Unlike what was found for EB, calculations on distorted isolated oligomers produced only a minimal $|\Delta\vec{\mu}|$. When the electron−hole screening arising from the fast dielectric response of the environment is included, geometric disorder leads to an average $|\Delta\vec{\mu}|$ of 1−4 D.

These results indicate that the origin of the $|\Delta\vec{\mu}|$ measured experimentally for MEH−PPV and the oligomers may be traced to a combination of inner-sphere disorder, arising from geometric distortion, and outer-sphere disorder, arising from internal fields applied by dipoles in the disordered glassy environment. Because $|\Delta\vec{\mu}|$ is predicted to be zero in the absence of symmetry breaking, electroabsorption measurements provide a facile and sensitive probe of the degree of disorder in these samples that may find applications, for instance, in screening materials.

Experimental Methods

Sample Preparation. Toluene and 2-methyltetrahydrofuran (MeTHF) were used to form organic glasses. Because fully dispersing the polymer in solvent is a slow process, we stirred the sample for 2 weeks before using. The sample was then placed between two ITO-coated glass slides separated by a Kapton tape spacer such that the thickness of the sample was 110 ± 4 μm. The optical density (OD) of the polymer glass samples was 0.01−0.19 (monomer unit concentration 10^{-4} to 2×10^{-3} M) and that of the oligomer was 0.01−0.55 (monomer unit concentration 10^{-4} to 5.5×10^{-3} M). The glasses were made by rapid immersion of the samples into an optical Dewar flask filled with liquid nitrogen. Transmission measurements using polarized light confirmed that the samples are isotropic (data not shown). We found it necessary to allow the polymer to dissolve in solution for over 2 weeks before it was sufficiently dispersed for us to make measurements on the sample.

Instrumentation. The electroabsorption apparatus is home-built and has been previously described in detail.[31] Briefly, it consists of a 0.3 m single monochromator (Spex) that disperses the light coming from a 150 W xenon arc lamp (Oriel) and gives a spectral resolution of 3−5 nm. The spectrally narrow light is then horizontally polarized with a Glan−Thomson polarizer to define the angle between the direction of polarization of the electric field of the incident light and the direction of the

electric field vector of the applied ac voltage. A 10^5-10^6 V/cm ac electric field on the sample was generated by a high-voltage power supply at 470 Hz. The transmitted light after passing through the sample was detected by a photodiode (UDT). Small changes in the OD of the sample due to the applied electric field were monitored with a lock-in amplifier. Low-temperature measurements were made using a liquid nitrogen Dewar (H. S. Martin). Steady-state fluorescence spectra were obtained using a Fluorolog-2 instrument (Spex) with 1 nm resolution in front-face geometry.

Data Fitting. The analysis of the electroabsorption data follows that in the literature.[32,33] The equations shown here are appropriate for the experimental conditions used, that is, the sample is embedded isotropically in a rigid glass. Essentially, the change in absorption due to the application of an external electric field is fit to the weighted sum of zeroth, first, and second derivatives of the zero-field absorption spectrum. The overall change in absorbance caused by the application of an electric field can be described by the following equation:

$$\Delta A(\tilde{\nu}) = \vec{\mathbf{F}}_{\text{eff}}{}^2\left[\mathbf{a}_\chi A(\tilde{\nu}) + \mathbf{b}_\chi \frac{\tilde{\nu}}{15\hbar}\left\{\frac{\partial}{\partial\tilde{\nu}}\left(\frac{A(\tilde{\nu})}{\tilde{\nu}}\right)\right\} + \mathbf{c}_\chi \frac{\tilde{\nu}}{30\hbar^2}\left\{\frac{\partial^2}{\partial\tilde{\nu}^2}\left(\frac{A(\tilde{\nu})}{\tilde{\nu}}\right)\right\}\right] \quad (1)$$

The term $A(\tilde{\nu})$ represents the unperturbed absorption as a function of frequency ($\tilde{\nu}$), and $\vec{\mathbf{F}}_{\text{eff}}$ represents the field at the sample in V/cm. This effective field includes the enhancement of the applied field due to the cavity field of the matrix. The subscript χ represents the angle between the direction of the applied electric field and the electric field vector of the linearly polarized light. The experiments reported here are performed at $\chi = 54.7°$ (magic angle). Note that magic angle is determined in the cell by taking into account the relevant indices of refraction as in ref 34. At $\chi = 54.7°$, the expressions of $\mathbf{a}_\chi$, $\mathbf{b}_\chi$, and $\mathbf{c}_\chi$ are related to the change in the transition moment polarizability (A_{ij}) and hyperpolarizability (B_{ijj}), the average change in the electronic polarizability ($\langle\underline{\Delta\boldsymbol{\alpha}}\rangle$), and the change in the dipole moments ($|\Delta\vec{\mu}|$), respectively, as given in eqs 2−4.

$$\mathbf{a}_{54.7} = \frac{1}{3|\vec{m}|^2}\sum_{i,j} A_{ij}{}^2 + \frac{2}{3|\vec{m}|^2}\sum_{i,j} m_i B_{ijj} \quad (2)$$

$$\mathbf{b}_{54.7} = \frac{10}{|\vec{m}|^2}\sum_{i,j} m_i A_{ij}\Delta\mu_j + \frac{15}{2}\langle\underline{\Delta\boldsymbol{\alpha}}\rangle \quad (3)$$

$$\mathbf{c}_{54.7} = 5|\Delta\vec{\mu}|^2 \quad (4)$$

In this work, we quote tr $\overleftrightarrow{\Delta\alpha}$, which represents the trace of the change in electronic polarizability between the ground and excited state (i.e., $\langle\underline{\Delta\boldsymbol{\alpha}}\rangle = {}^1/_3$ tr $\overleftrightarrow{\Delta\alpha}$) to be consistent with the bulk of published work in the area of Stark spectroscopy on polymers. Information regarding $|\Delta\vec{\mu}|$ for the molecule is contained in the $\mathbf{c}_{54.7}$ term (eq 4). It is important to emphasize that, for an isotropic sample such as those studied in this work, only the magnitude and not the sign of $\Delta\vec{\mu}$ is measured. In the above equations, the tensors $\underline{A}$ and $\underline{B}$ represent the transition polarizability and hyperpolarizability, respectively. These describe the effect of $\mathbf{F}_{\text{eff}}$ on the molecular transition moment: $\vec{m}(\vec{\mathbf{F}}_{\text{eff}}) = \vec{m} + \underline{A}\cdot\vec{\mathbf{F}}_{\text{eff}} + \vec{\mathbf{F}}_{\text{eff}}\cdot\underline{\underline{B}}\cdot\vec{\mathbf{F}}_{\text{eff}}$. These terms are generally small for allowed transitions and can therefore be neglected relative to other terms in the expression for $\langle\underline{\Delta\boldsymbol{\alpha}}\rangle$ (eq 3).

SCHEME 2[a]

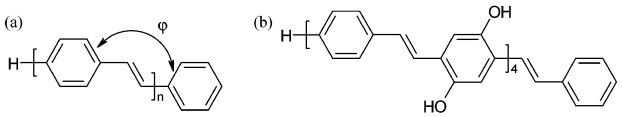

[a] (a) The repeat unit of PPV showing the definition of the dihedral angle between the phenylene rings (φ). (b) The model OPPV-9 oligomer with hydroxy substitution.

The coefficients, $\mathbf{a}_\chi$, $\mathbf{b}_\chi$, and $\mathbf{c}_\chi$, are extracted by means of a linear least-squares (LLSQ) fit of the electroabsorption signal to the sum of the derivatives of $A(\tilde{\nu})$. If the resultant fit to the absorption line shape (a single set of $\mathbf{a}_\chi$, $\mathbf{b}_\chi$, and $\mathbf{c}_\chi$) is *not* of high quality, this is an indication that there is more than one transition (electronic or vibronic) underlying the absorption band, each having different electrooptical properties. Our fitting strategies are described in ref 35.

Computational Methods

Geometry Optimization and Introduction of Inner-Sphere Disorder. The two types of oligomers studied computationally are shown in Scheme 2. The first (Scheme 2a) is the unsubstituted PPV, while the second (Scheme 2b) has hydroxyl groups attached to every other ring so as to resemble the substituted oligomer studied experimentally, OPPV-9 (Scheme 1b). Planar oligomers of PPV with 2−16 rings were constructed to study the chain-length dependence of the electrooptical properties. To determine the effect of chain conformation on the electronic properties of these species, nonplanar geometries of an 8-ring PPV oligomer (PPV-8), were obtained by constraining the dihedral angles (φ in Scheme 2a) between adjacent phenylene rings while optimizing all other coordinates. Ten nonplanar structures were created having dihedral angles between −45° and +45° that were generated by a uniform random number generator. This geometry distortion is defined as the inner-sphere disorder in this paper.

All of the geometry optimizations were performed using MOPAC 7 with the AM1 Hamiltonian.[36] Following optimization, the inertial axes for each structure were used to define a coordinate system for the calculation of the polarizabilities. These were defined such that the moments of inertia along the *X*, *Y*, and *Z* axes increase in magnitude and the origin lies at the center of mass. In the linear and planar structure, this corresponds to the *X* axis lying along the long dimension of the molecule and the *Y* axis being in the molecular plane.

Electronic Structure Calculations. All calculations reported in this paper were performed at the INDO/SCI level. A recently developed direct CI method was applied that permits inclusion of single excitations between all molecular orbitals (full SCI).[37] Full SCI was used for all calculations except for those in which a PPV oligomer was surrounded by a random dipole lattice (see below). In this case, because of the need to construct hundreds of different lattices to obtain a statistical distribution of the electrooptical properties, the associated INDO/SCI calculations included only π and π^* orbitals of the planar PPV-8 oligomer. For planar PPV, the primary effect of restricting the SCI calculation to π orbitals is to increase the $1B_u-mA_g$ energy separation by ∼0.2 eV. This is corrected by changing the dielectric screening parameter (see below).

Finite-Field Method for Electrooptical Property Calculations. The finite field method, described by Kurtz et al.,[38] was used to calculate the dipole moments and polarizabilities of the ground and excited states. The magnitude of the applied electric field used was 5×10^5 V·cm^{-1} or 9.7×10^{-5} au. Use of a

field strength that is too large or too small causes numerical errors that make the calculated results unstable (see Supporting Information). The value chosen here leads to stable numerical results and is also of the same magnitude as the external field used in the experiments reported here.

Both the energy derivative method, which obtains the dipole and polarizability from derivatives of the energy, and the dipole moment derivative method, which obtains the polarizability from derivatives of the induced dipole moment, were tested. Although, in most cases, the results obtained with these two methods were very similar, we found that the dipole moment derivative method was more stable both with regard to the magnitude of the finite field used to evaluate the derivatives and with regard to truncation of the molecular orbitals included in the SCI calculation (see Supporting Information). Therefore, in this paper, only the dipole moment derivative results are reported.

Dielectric Screening Model for Inclusion of Solvation Effects. Dielectric screening effects are included in the calculation to obtain reasonable results for the higher energy excited states, especially the $m\mathrm{A_g}$ state that plays an important role, as we will demonstrate, in establishing the magnitude of the excited-state polarizability. Moore et al.[20] compared a dynamic dielectric model, which explicitly includes the time scales of both the electron−hole motion and the dielectric response, with a simpler fast dielectric model, which assumes that the dielectric polarization can follow the electron−hole motion and screen their interaction. This comparison indicated that the fast dielectric model provides a reasonable description of the effects of dielectric screening on the excited states, and it is this model that is used throughout this paper.

The fast dielectric model is implemented by first transforming from the delocalized, canonical Hartree−Fock orbitals to local orbitals that are centered on particular molecular segments. This is done by using the local orbital method of Pasquinelli,[39] with the segments of the PPV oligomer being chosen as the individual phenylene and vinylene groups. In these localized orbitals, the singly excited configurations of SCI theory contain an electron and hole, each of which is centered on a particular phenylene or vinylene group of the oligomer. The diagonal elements of the SCI Hamiltonian matrix represent the energy of each particular arrangement of the electron and hole, and dielectric screening is included by adding a dielectric stabilization energy to each of these diagonal elements.

The dielectric stabilization (or solvation) energy is obtained as follows. Within a linear dielectric approximation, the solvation energy of an arbitrary charge distribution may be written as

$$E_{\mathrm{solv}} = \sum_{i,j}^{N} \rho_i \rho_j G(\mathbf{r}_i,\mathbf{r}_j) \tag{5}$$

where ρ_i is the charge density at site i and the Green's function, $G(\mathbf{r}_i,\mathbf{r}_j)$, describes the energy of interaction between a unit charge at $\mathbf{r}_i$ and the polarization induced by a unit charge at $\mathbf{r}_j$. Here, we assume that the Green's function depends only on the distance between the two points, $|\mathbf{r}_i - \mathbf{r}_j|$. For large $|\mathbf{r}_i - \mathbf{r}_j|$, a continuum dielectric model gives

$$G(\mathbf{r}_i,\mathbf{r}_j) = \frac{1}{2}\left[\frac{1-\epsilon}{\epsilon}\right]\frac{1}{|\mathbf{r}_i - \mathbf{r}_j|} \tag{6}$$

where ϵ is the dielectric constant of the material. Because organic systems typically have low optical dielectric constants, $\epsilon = 2.0$ was used in the calculations presented here. The short-range behavior of $G(\mathbf{r}_i,\mathbf{r}_j)$ is evaluated explicitly for point charges surrounded by polyacetylene chains, each of which is modeled at the Hückel level,[20] and this function is spliced with that of eq 6 to obtain a smooth function of $|\mathbf{r}_i - \mathbf{r}_j|$ (see Supporting Information). This approach provides a function that interpolates in a reasonable manner between $G(0)$, the solvation energy of a point charge (−1.1 eV for the function used here), and the form of eq 6 for distances greater than about 6 Å. While this is a reasonable function for $G(\mathbf{r}_i,\mathbf{r}_j)$, it may not be quantitative, so we introduced a semiempirical scaling parameter, S_{diel}, that is multiplied by $G(\mathbf{r}_i,\mathbf{r}_j)$ and sets the strength of the dielectric screening. Below, S_{diel} is adjusted on the basis of the experimentally observed energy of the $m\mathrm{A_g}$ state, which is ~0.6 eV above the $1\mathrm{B_u}$ state.[40,41] Inclusion of σ orbitals alters the gap between the $1\mathrm{B_u}$ and $m\mathrm{A_g}$ states, such that a 0.6 eV gap between the $1\mathrm{B_u}$ and $m\mathrm{A_g}$ states is obtained for $S_{\mathrm{diel}} = 1.4$ in full SCI and for $S_{\mathrm{diel}} = 1.0$ when only π orbitals are included in the SCI basis. These values for S_{diel} are used in the remainder of the paper.

Models for Outer-Sphere Disorder. The dielectric screening discussed in the previous section models the effects of optical polarization on the electron−hole interaction in the excited states. This effect results from the dynamic polarization induced in the solvent molecules by the electron and hole. In this section, we consider a quite different effect, that of symmetry breaking due to the permanent charges on the solvent molecules and the amorphous arrangement of these solvent molecules. Such environmental effect is defined as the outer-sphere disorder in the paper. Results are presented for the following two models.

A. Explicit Small Molecules as the Environment. In this model, molecular mechanics is used to surround a PPV-8 oligomer that is constrained to remain in an ideal planar geometry with an amorphous sample of MeTHF molecules. The charges on the MeTHF were Mulliken charges obtained from an AM1 calculation on an isolated MeTHF molecule. The amorphous structure was obtained by running a molecular dynamics trajectory and quenching the sample at four different times (see Supporting Information for details). The resulting charge distribution was then used to calculate the potential applied to the PPV-8 structure using Coulomb's law,

$$\boldsymbol{V}_a = \frac{1}{4\pi\epsilon_0}\sum_{i}^{N}\frac{q_i}{|\mathbf{r}_a - \mathbf{r}_i|} \tag{7}$$

where V_a is the potential for atom a at $\mathbf{r}_a$ and q_i is a charge at $\mathbf{r}_i$ in this random charge distribution with a total of N charges. While these calculations do give some insight into the effects of an amorphous environment, visual examination of the lattices shows unphysically large density fluctuations (i.e., voids). This is because the calculations were not performed at constant pressure. To avoid this complication and to permit the examination of a large number of lattices in a computationally efficient manner, the dipole lattice model, described in the next section, was developed.

B. Dipole Lattice Model of Random Environment. A lattice was constructed containing a cavity for planar PPV-8 in which each lattice site was occupied by a randomly oriented dipole. The orientations of the dipoles were obtained from a random number generator to generate the polar angles θ (using a $\sin\theta$ distribution) and ϕ (using a uniform distribution). The cavity size, the number of dipoles in the lattice, the magnitude of the dipoles, and the spacing between the lattice sites were param-

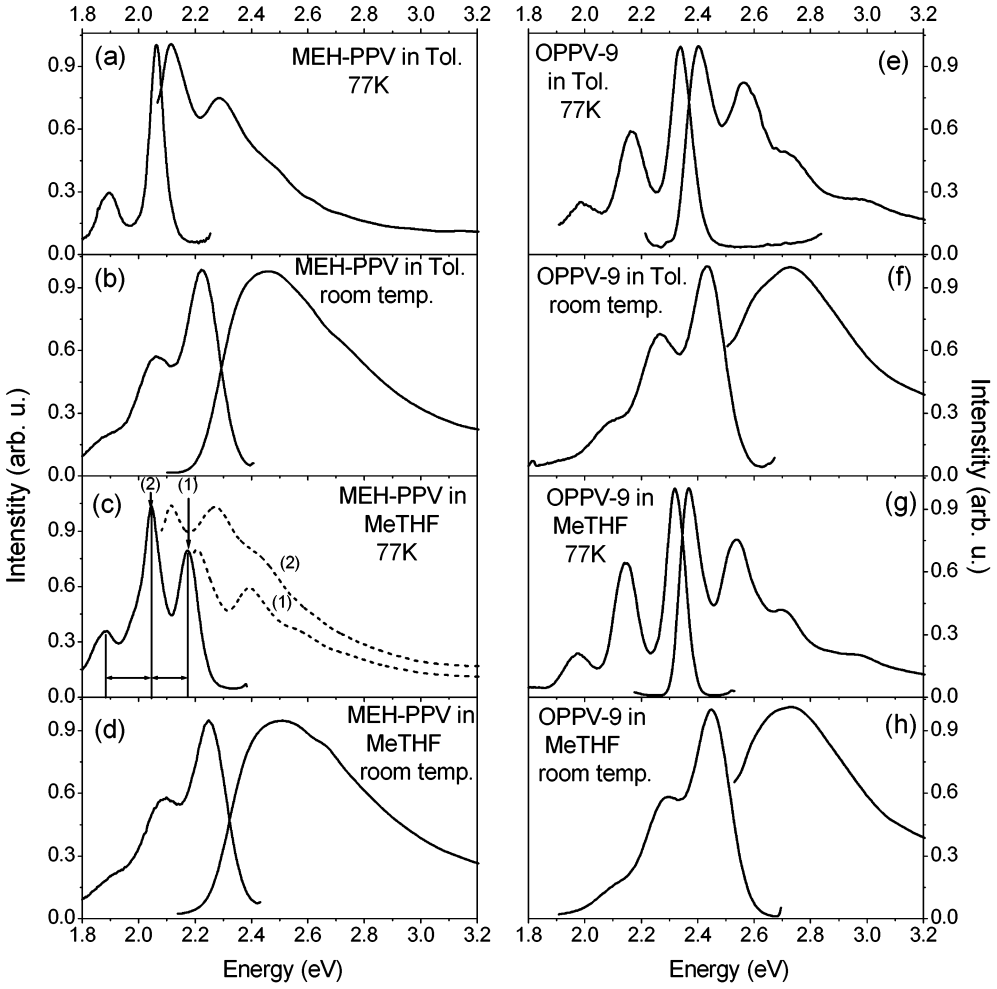

Figure 1. Fluorescence and fluorescence excitation spectra of MEH−PPV and OPPV-9 dispersed in toluene and MeTHF measured at 77 K and room temperature, as indicated in the insets. Intensities have been normalized for better comparison. MEH−PPV in MeTHF at 77 K shows an unequal spacing between the fluorescence peaks. Excitation spectra 1 and 2 correspond to collection wavelengths of 573 and 608 nm, respectively, which are designated on the emission spectrum.

eters that were varied in building and testing the dipole lattice model. The dependence of the electrooptical properties on these lattice parameters is discussed in detail in the Supporting Information.

In the main text, we report calculations performed using two types of lattices. The first lattice models the overall dipole moment of the solvent molecules. This lattice has a spacing of 6 Å, which is similar to the size of MeTHF, and dipoles with magnitude 1.5 D, which is that calculated for a MeTHF molecule using AM1. The cavity is such that the spacings between the outmost hydrogen atoms in the PPV-8 and the closest lattice sites are 4.5, 3.5, and 6 Å in the *X*, *Y*, and *Z* directions, respectively. Results were generated for 500 randomly generated lattices.

The second lattice reported in the main text models CH bond dipoles. In Kohler's studies of octatetraene entrained in *n*-alkane matrixes, in which the alkane molecules of the matrix have no net dipole, significant internal fields were found to arise from the CH bond dipoles.[29,30] To model the CH dipoles of the glass within the random lattice approach, we used a lattice with the same cavity size as that of the first lattice but with a lattice spacing of 3 Å and dipoles of 0.65 D, the dipole moment of a CH_2 group. These lattice parameters give results that are similar to those of the first lattice.

Results and Discussion

Fluorescence Spectra in Organic Glasses. To examine the effect of the frozen glass matrix on the properties of the oligomers and of MEH−PPV, their fluorescence excitation and dispersed fluorescence spectra in toluene at room temperature and at 77 K were obtained (Figures 1 and 2). The spectra of MEH−PPV and OPPV-9, in addition, were obtained in MeTHF glass (Figure 1). In all cases, the excitation spectra at 77 K are substantially narrower than those at room temperature and the Stokes shift is significantly smaller. Moreover, reasonable mirror-image symmetry is observed in the glass for all systems, though, for MEH−PPV in MeTHF, it is apparently obscured by the presence of multiple conformers within the glass matrix (see below). Both the narrowing of the spectra and the decrease in the observed Stokes shift upon formation of the glass are likely to be the result of decreased excitation of low-frequency torsional modes at low temperature.[42−45]

As noted previously, the emission spectrum of MEH−PPV in MeTHF is complicated by the presence of at least two spectrally distinct species. Unlike what is seen in toluene, the spacings between the three most prominent bands in the emission spectrum (solid line, Figure 1c) of MEH−PPV in MeTHF are irregular, suggesting that they do *not* constitute a vibronic progression. Moreover, two excitation spectra having

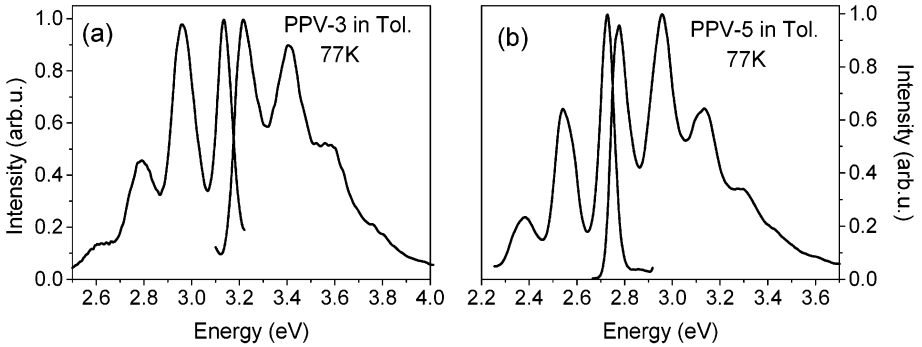

Figure 2. Fluorescence and fluorescence excitation spectra of PPV-3 and PPV-5 dispersed in toluene measured at 77 K. Intensities have been normalized for better comparison.

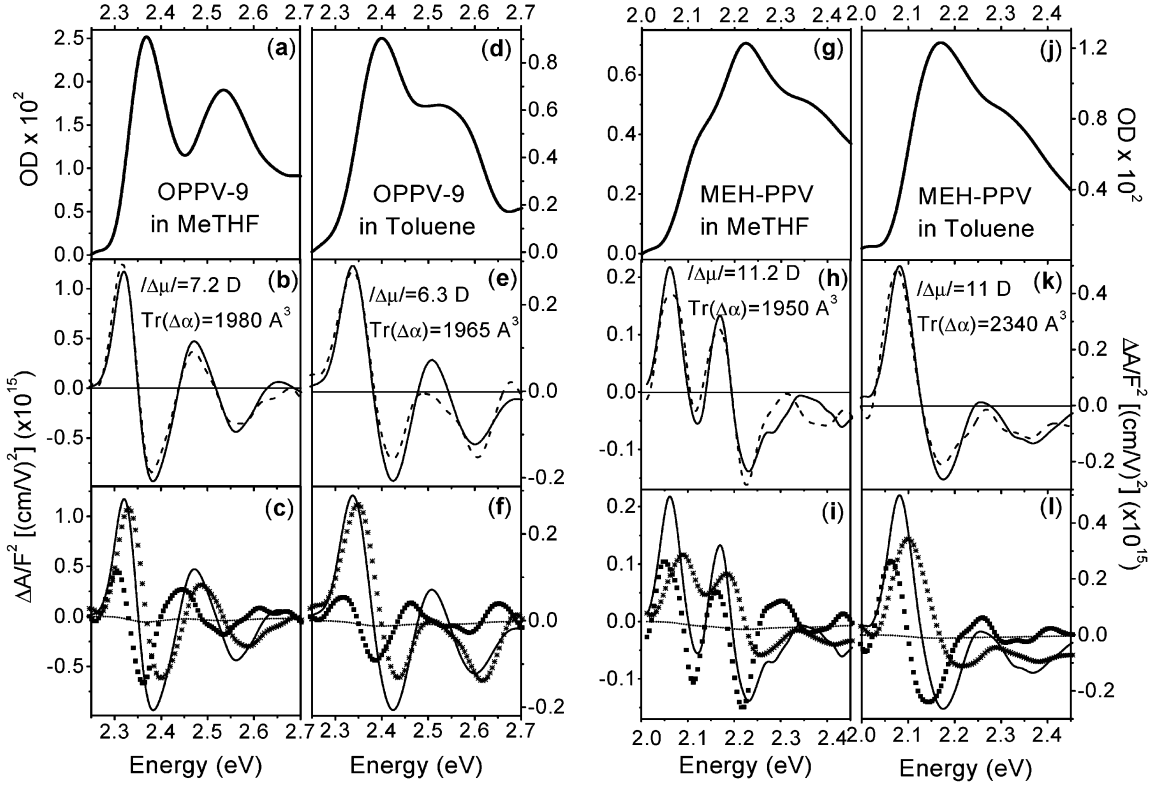

Figure 3. Absorption (top panels) and electroabsorption spectra (middle panels, solid line) of OPPV-9 and MEH−PPV dispersed in glassy MeTHF and toluene. The fits to the electroabsorption spectra are also shown in the middle panels (dashed lines), along with the parameters derived from the fit. In the lower panels, the zeroth (●), first (∗), and second (■) derivatives of the absorption spectra are shown together with the electroabsorption spectra (solid lines). The MEH−PPV in MeTHF spectrum was obtained at 0.07 mM polymer concentration; the MEH−PPV in toluene was obtained at 0.122 mM polymer concentration. The oligomer spectrum was obtained at 0.091 mM in toluene and 0.25 mM in MeTHF.

different vibronic spacings from one another (dashed line spectra, labeled 1 and 2, respectively, in Figure 1c) are obtained upon excitation of each of the two bands at lowest energy (labeled 1 and 2 in the solid line spectrum, Figure 1c). From this, we conclude that the two most intense bands in the MEH−PPV spectrum in MeTHF glass represent the respective origins of two distinct conformers of the polymer. It is interesting to note that Barbara and co-workers have identified two distinct conformers of MEH−PPV dispersed in inert polymer matrixes such as polystyrene using single-molecule fluorescence spectroscopy.[46]

Electroabsorption Spectra in Organic Glasses. Figure 3 contains the absorption and the electroabsorption spectra of the lowest energy band of OPPV-9 and MEH−PPV dispersed in toluene and in MeTHF at 77 K. The middle row shows the electroabsorption spectra (solid line) and fit (dashed line), while the bottom row contains the decomposition of the fits into the zeroth, first, and second derivatives of the corresponding absorption spectrum (see Experimental Methods). These measurements were made in the low concentration limit (OD of ∼0.01 in a path length of ∼110 μm), which corresponds to monomer unit concentration of about 10^{-4} M. We therefore expect that these results at low concentrations can be meaningfully compared to the time-resolved microwave conductivity (TRMC) results of Warman et al. that were obtained in dilute room-temperature solution (10^{-4} M in monomer units).[18,47]

High-quality fits to the electroabsorption spectrum are observed for both the oligomer and the polymer in both solvent glasses. These fits yield similar values of tr $\overleftrightarrow{\Delta\alpha}$ for OPPV-9 as for the polymer, though the change in dipole moment is somewhat smaller for the oligomer (6.3 D) than for the polymer (11 D).

As noted earlier for the fluorescence spectra, the identity of the solvent has a dramatic effect on the appearance of the

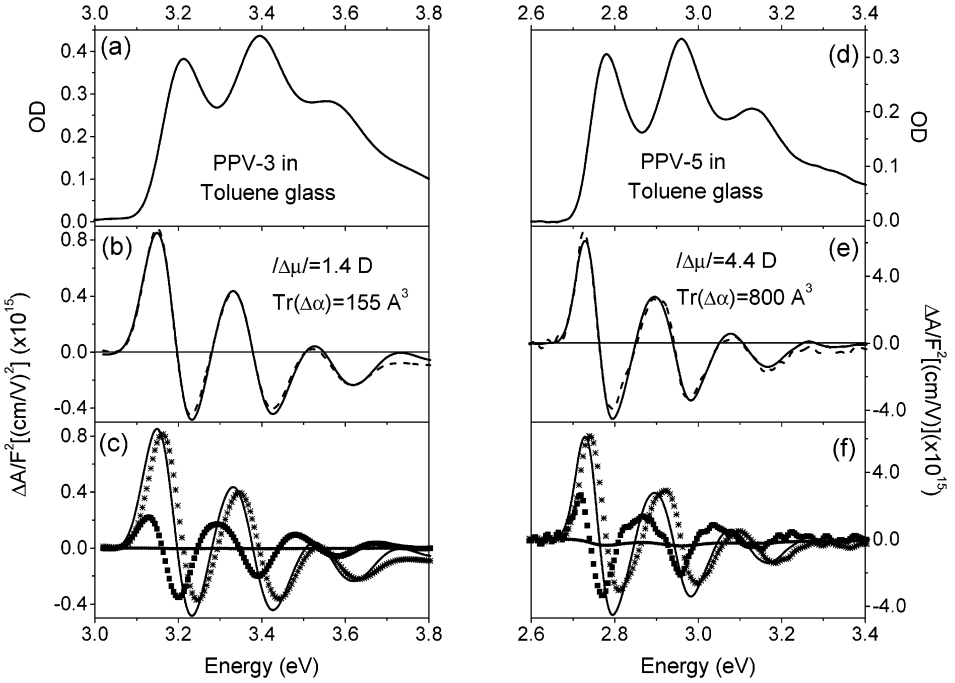

Figure 4. Absorption (a, d) and electroabsorption spectra (b, e) of PPV-3 and PPV-5, respectively, dispersed in glassy toluene. The fits to the electroabsorption spectra are shown with dashed lines in panels b and e, and the parameters derived from each fit are given in the inset of the panel. The zeroth (●), first (∗), and second (■) derivatives of the absorption spectra are shown together with the electroabsorption spectra (solid lines) in the lower panels. The PPV-5 spectrum was obtained at 3.3 mM and the PPV-3 spectrum at 4.33 mM concentrations.

polymer absorption spectrum, though not on that of OPPV-9. In toluene glass, both the oligomer and the polymer exhibit a vibronic progression with a spacing of ∼1350 cm^{-1} with that in the oligomer being more highly resolved (compare panel d to panel j in Figure 3). In MeTHF glass, the oligomer exhibits a similar progression to that seen in the toluene glass (Figure 3a), while the absorption spectrum of the polymer is significantly altered (Figure 3g). Specifically, the spacing between the first two peaks in the polymer spectrum (seen most readily in the electroabsorption spectrum, Figure 3h) is ∼1000 cm^{-1}, while that between the second and third peaks is ∼1350 cm^{-1}. The irregularity in these spacings suggests that more than one species of MEH−PPV is present in the MeTHF glass though similar heterogeneity is not evident in the toluene glass. This confirms the interpretation of the fluorescence spectrum of this sample given previously.

Despite this apparent heterogeneity in the MEH−PPV sample in MeTHF, the overall fit to the electroabsorption spectrum is of reasonably high quality, at least in the low concentration limit. However, as the concentration of MEH−PPV is increased, the experimental data and the fit deviate substantially in MeTHF (data not shown), suggesting that these different species may have different values of tr $\overleftrightarrow{\Delta\alpha}$ or $|\Delta\vec{\mu}|$ or both. Another possible explanation is that aggregates are formed at higher concentration and these have different values of tr $\overleftrightarrow{\Delta\alpha}$ or $|\Delta\vec{\mu}|$ or both than the isolated species.

Turning now to the electroabsorption results for the PPV oligomers (Scheme 1c,d), shown in Figure 4, we find that the fits to the data are of exceptionally high quality, suggesting that all possible conformers present and all of the vibronic levels have similar electrooptical parameters. As expected, the values obtained for tr $\overleftrightarrow{\Delta\alpha}$ of these shorter oligomers (780 Å for PPV-5 and 140 Å for PPV-3) are smaller that those obtained for the 9-ring substituted oligomer. The values of $|\Delta\vec{\mu}|$ are also somewhat smaller than those obtained for the longer chain length species, consistent with a mechanism in which the dipole moment is induced by interaction of the molecular polarizability with a disordered local field (see below).

Comparison to Other Literature Results. The results obtained here for tr $\overleftrightarrow{\Delta\alpha}$ of MEH−PPV lie within the range of values that have been reported earlier (∼400−20 000 $Å^3$) for both MEH−PPV and PPV also using electroabsorption.[41,48,49] This variation may in part reflect differences in sample conditions, that is, solvent glass versus neat film. It is particularly interesting to compare our findings with the microwave conductivity measurements of Warman et al.[18,47] obtained for the oligomer and the polymer in dilute room-temperature toluene because these two techniques probe different regions of the excited-state surface. Because electroabsorption probes the Franck−Condon region, it is sensitive to the presence of a distribution of ground-state conformations having different effective conjugation lengths. Normally, solid-state or frozen-glass samples are used as well. Microwave conductivity, on the other hand, measures the properties of the *relaxed* excited state in a liquid-phase sample.

Microwave conductivity gives somewhat larger values of tr $\overleftrightarrow{\Delta\alpha}$ (∼3000 $Å^3$ for the oligomer and ∼4800 $Å^3$ for the polymer) than those reported here (Table 1). A somewhat larger discrepancy is seen when we compare our results for PPV-3 and PPV-5 (Table 1) to those obtained from microwave conductivity, which are ∼1100 and ∼2800 $Å^3$, respectively.[18] One may expect a discrepancy to arise in the case of the polymer because microwave conductivity measures the properties of the system presumably after rapid intramolecular energy transfer to the longest segment has occurred. However, to explain differences between the results obtained on the oligomer using the two methods, it may be necessary to consider the effects of the environment (glass versus solution) or the characteristics of the region of the excited state surface being probed or both.

TABLE 1: Parameters Obtained from Absorption, Emission, and Electroabsorption Spectra

molecule	solvent/T (K)	A_{max} of 0−0, 0−1 bands[a]	emission max of 0−1, 0−1 bands[a]	tr $\overleftrightarrow{\Delta\alpha}$[c]	$\lvert\Delta\vec{\mu}\rvert$[d]
MEH−PPV	MeTHF/298	2.490	2.250, 2.087		
	MeTHF/77	*b*	*b*	2000 ± 200	11 ± 1
	toluene/298	2.450	2.226, 2.066		
	toluene/77	2.119, 2.291	2.066, 1.895	2300 ± 200	11 ± 2
OPPV-9	MeTHF/298	2.710	2.450, 2.283		
	MeTHF/77	2.371, 2.539	2.318, 2.146	2000 ± 200	7.2 ± 1.0
	toluene/298	2.720	2.432, 2.266		
	toluene/77	2.404, 2.571	2.339, 2.168	2000 ± 200	6.3 ± 0.8
PPV-5	toluene/77	2.780, 2.959	2.725, 2.546	780 ± 80	4.4 ± 0.5
PPV-3	toluene/77	3.207, 3.391	3.133, 2.952	140 ± 20	1.8 ± 0.4

[a] In eV. Errors are ±0.003 eV. [b] Indicates the presence of overlapping transitions (see text). [c] In Å^3. [d] In D.

The latter possibility is currently being investigated via electrofluorescence measurements in organic glasses.

More relevant from the point of view of this study is that the substantial values of $|\Delta\vec{\mu}|$ that we measure for MEH−PPV and for both the substituted and unsubstituted oligomers have no precedent in the literature, either in electroabsorption or microwave conductivity studies. However, using electroabsorption, Hovárth et al. have reported a $|\Delta\vec{\mu}|$ of 50 D for a disordered polydiacetylene film having an estimated average polarizability of ∼7000 Å^3 (tr $\overleftrightarrow{\Delta\alpha}$ of ∼21 000 Å^3).[28] Whether a value for $|\Delta\vec{\mu}|$ is reported for MEH−PPV in any given study may be attributed to differences in data interpretation that are summarized below. In this contribution, *we will argue that it is valid to associate this second-derivative contribution to the field response in the organic glass matrixes with a nonzero effective* $|\Delta\vec{\mu}|$ *that is induced by disordered matrix fields*.

Models for the Origin of a Non-zero $|\Delta\vec{\mu}|$. Similar to what is found here for MEH−PPV and the oligomers, numerous other studies in the literature have also reported substantial values of $|\Delta\vec{\mu}|$ for all-trans polyenes, as well as for longer (up to polymeric) conjugated species.[23−26,28,29] In all cases, the molecules studied are *nominally* symmetric (C_{2h}-derived) and would therefore be predicted to have a $|\Delta\vec{\mu}|$ that is close to zero.

Two frequently invoked mechanisms for the required symmetry breaking are the following. One is that structural disorder (torsions, etc.), possibly induced by the surrounding matrix, can lead to a reduction in the effective point group of the molecule. Weiser and co-workers observed a ∼50 D dipole moment in disordered samples of polydiacetylene but not in ordered crystalline samples.[28] They attributed the large dipole to defects in the disordered sample and suggested that these defects break the centrosymmetry of the exciton state by imposing asymmetric boundary conditions on the exciton wave function. The second symmetry breaking mechanism is the presence of asymmetric fields in the local condensed-phase environment, which will induce a substantial $|\Delta\vec{\mu}|$ in molecules having a significant $\overleftrightarrow{\Delta\alpha}$.[22,50]

A third model, recently outlined by Vardeny et al., is that a second-derivative contribution to the fit to the electroabsorption spectrum can arise from having a variety of effective conjugation lengths in a given sample of a long-chain polyene, all of which have different values of tr $\overleftrightarrow{\Delta\alpha}$.[41] Fitting such a heterogeneous sample using the formalism commonly used to model electroabsorption data (see Experimental Methods) can lead to the observation of higher (second) derivatives that are then *incorrectly* ascribed to a characteristic molecular $|\Delta\vec{\mu}|$. An upper limit of this contribution to the second derivative of the EA spectrum can be obtained by assuming that regions with short conjugation length, on the blue side of the absorption line, have zero tr $\overleftrightarrow{\Delta\alpha}$.

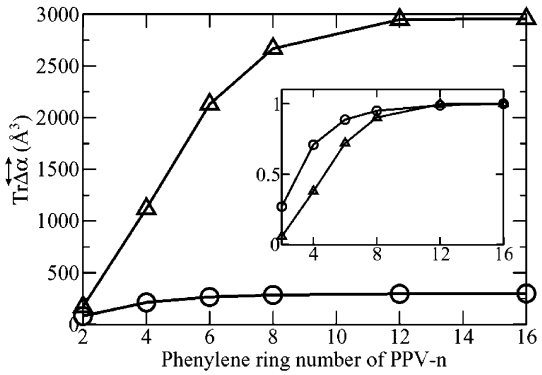

Figure 5. Chain length dependence of the polarizability change tr $\overleftrightarrow{\Delta\alpha}$ calculated for planar PPV-*n* oligomers in the gas phase (○) and with the inclusion of dielectric screening (△). The dielectric screening parameter S_{diel} is set at 1.4 such that for longer chains the $1B_u-mA_g$ energy separation is ∼0.6 eV. The inset shows the ratio of tr $\overleftrightarrow{\Delta\alpha}$(PPV-*n*) to tr $\overleftrightarrow{\Delta\alpha}$(PPV-16) to illustrate the rate at which tr $\overleftrightarrow{\Delta\alpha}$ approaches the long chain limit.

If this were the case, only the red side of the absorption line would shift in the applied field and the observed broadening of the line would be roughly twice the observed red shift. A useful benchmark is to consider the value of $|\Delta\vec{\mu}|$ that would arise from interpreting a broadening that is twice the observed red shift in terms of a $|\Delta\vec{\mu}|$. This can be obtained by dividing the observed tr $\overleftrightarrow{\Delta\alpha}$ by the applied external field of about 3×10^5 V/cm, which gives a value of 2 D. This is a small fraction of the broadening that we observe, which corresponds to 6−10 D. This indicates that this third mechanism, by which the dependence of the polarizability on conjugation length leads to a broadening of the spectral line in an applied field, can only account for a small portion of the observed broadening.

In another model, Martin et al. have suggested that the electroabsorption signal of nominally symmetric polyenes deviates from the pure first-derivative line shape expected for a field response dominated by tr $\overleftrightarrow{\Delta\alpha}$ because of the contribution of a bleach signal in the higher-energy region.[51] This bleach is attributed to intensity borrowing from the $1B_u$ state by an even-parity state that becomes allowed in the presence of the applied field. This model does not appear to match our results, particularly for the oligomers, because all of our electroabsorption line shapes deviate from the first derivative of the absorption spectra more or less equally across the entire frequency range probed (Figures 3 and 4, bottom panels). We will therefore not consider it further here.

The computational results presented below address the first two models described above. Specifically, two mechanisms for inclusion of symmetry breaking are examined here: (1) inner-sphere disorder or geometric distortion of the molecule in a dielectric medium and (2) outer-sphere disorder or inclusion of a random dipole field surrounding a symmetric molecule that mimics the solvent glass. Our results suggest that both types of disorder, in conjunction with dielectric screening, may contribute significantly to the observed $|\Delta\vec{\mu}|$, the contribution due to the random dipole field being somewhat larger. We note that *neither* mechanism will lead to a significant $|\Delta\vec{\mu}|$ if the effects due to dielectric screening are not also accounted for.

Computational Results

Predictions for tr $\overleftrightarrow{\Delta\alpha}$. Figure 5 shows the chain length dependence of tr $\overleftrightarrow{\Delta\alpha}$ for planar oligomer structures of PPV-*n* obtained with and without inclusion of dielectric screening. The

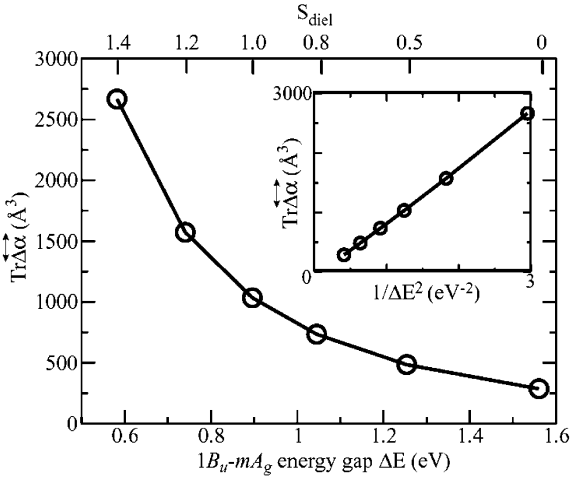

Figure 6. The value of tr $\overleftrightarrow{\Delta\alpha}$ for a planar and linear PPV-8 oligomer as a function of the strength of the dielectric medium. The upper axis shows the solvation scaling factor, S_{diel}, and the lower axis shows the $1B_u-mA_g$ energy separation (ΔE). The inset illustrates the linear relationship between tr $\overleftrightarrow{\Delta\alpha}$ and $1/\Delta E^2$.

value of tr $\overleftrightarrow{\Delta\alpha}$ saturates by $n \approx 8$, in accordance with other studies.[18,52−55] However, the gas-phase tr $\overleftrightarrow{\Delta\alpha}$ value is only ∼300 Å^3 for long-chain oligomers, which is *considerably smaller* than the experimentally observed values of Table 1. However, inclusion of dielectric screening (shown in Figure 5 by the triangles) via the fast dielectric model (see Experimental Methods) increases the predicted tr $\overleftrightarrow{\Delta\alpha}$ to be roughly 10 times the value from the gas-phase calculation, leveling off at around 3000 Å^3 for long chains. This produces a significantly better match to experiment (Table 1). A similar situation arises in density functional theory calculations of excited-state polarizabilities, in which addition of dielectric screening of electron−hole interactions leads to a good match between theory and experiment.[56] The inset of the figure shows that tr $\overleftrightarrow{\Delta\alpha}$ approaches the long chain limit more quickly in the gas-phase calculations than in those including dielectric screening, but in either case, tr $\overleftrightarrow{\Delta\alpha}$ is near the long chain limit by eight rings.

The PPV-8 oligomer was studied in greater detail, and Figure 6 shows the calculated tr $\overleftrightarrow{\Delta\alpha}$ as the scaling factor for the dielectric interaction is increased from $S_{diel} = 0$ (gas phase) to $S_{diel} = 1.4$. The top axis of the graph shows S_{diel} while the lower axis represents the calculated energy difference between the $1B_u$ and mA_g states. Figure 6 indicates that the experimental energy difference (0.55−0.65 eV) is obtained with a value of S_{diel} lying between 1.32 and 1.44. This value of S_{diel} in turn places tr $\overleftrightarrow{\Delta\alpha}$ between 2100 and 3000 Å^3. A similar result is obtained for the OPPV-9 oligomer (Supporting Information), which is in excellent agreement with the experimentally observed value (Table 1).

The dependence of tr $\overleftrightarrow{\Delta\alpha}$ on the $1B_u-mA_g$ energy gap can be understood as follows. The tr $\overleftrightarrow{\Delta\alpha}$ is dominated by the component along the long axis of the oligomer, $\Delta\alpha_{xx}$. In this direction, assuming the excited-state polarizability is dominated by the transition moment between the $1B_u$ and the mA_g state, the polarizability change, $\Delta\alpha_{xx}$, can be written as

$$\Delta\alpha_{xx} \approx \frac{|\langle 1B_u|\mu_x|mA_g\rangle|^2}{\Delta E} \qquad (8)$$

If we further assume that the oscillator strength between the $1B_u$ and mA_g states is a constant, the transition moment has the following dependence on the energy gap:

$$|\langle 1B_u|\mu_x|mA_g\rangle|^2 \propto \frac{1}{\Delta E} \qquad (9)$$

The dependence of eq 9 results from the definition of the oscillator strength as the product of ΔE and the square of the transition moment. With these assumptions, tr $\overleftrightarrow{\Delta\alpha}$ should be inversely related to the square of ΔE. The inset of Figure 6 shows that this is indeed the case for the calculations performed here.

TABLE 2: Calculated Electrooptical Properties for 10 Randomly-Distorted PPV-8 Structures

	disordered PPV-8 structures[a]		linear and planar PPV-8	
	gas phase	solvated[b]	gas phase	solvated[b]
ΔE^c (mA_g-1B_u)	1.552 ± 0.004	0.62 ± 0.01	1.561	0.58
tr $\overleftrightarrow{\Delta\alpha}^d$	264 ± 5	2000 ± 100	285	2668
$\lvert\Delta\vec{\mu}\rvert^e$	0.04 ± 0.02	4 ± 1	0.00	0.02
$E_{1B_u}{}^c$	2.98 ± 0.02	2.38 ± 0.03	2.873	2.237

[a] The numbers in this column represent the average values and standard deviations for a set of 10 randomly generated geometrically disordered structures of PPV-8 (see text). [b] For solvated calculations, the dielectric scaling factor is 1.4 (see text). [c] In eV. [d] In Å^3. [e] In D.

Effect of Inner-Sphere Disorder (Chain Conformation) on Electronic Properties. Table 2 contains the values of tr $\overleftrightarrow{\Delta\alpha}$ obtained for 10 oligomers of PPV-8 with dihedral angles between adjacent phenylene rings assigned randomly within the range −45° to +45°. The tr $\overleftrightarrow{\Delta\alpha}$ values for all structures are slightly smaller than that of a planar PPV-8 oligomer. Specifically, the values of tr $\overleftrightarrow{\Delta\alpha}$ are ∼90% of that of the planar structure without inclusion of dielectric screening and ∼80% of that with screening. In contrast, the predicted excitation energy of the lowest energy electronic transition is quite sensitive to chain conformation, with the average 0−0 energy in the 10 random PPV-8 structures being ∼0.14 eV (1100 cm^{-1}) higher than that of the planar geometry.

More interesting is the fact that the average $|\Delta\vec{\mu}|$ of the 10 structures is nearly zero without the inclusion of dielectric screening but increases to 4 ± 1 D with screening. The larger $|\Delta\vec{\mu}|$ obtained with the inclusion of screening can be understood as follows. For a symmetric structure, the electron and hole are symmetrically distributed in the excited state. The calculated $|\Delta\vec{\mu}|$'s are a measure of how geometric distortions break this electronic symmetry. Screening weakens the attraction between the electron and hole, increasing the degree of electronic symmetry breaking. The above results suggest that loss of C_{2h} symmetry in the oligomer structure itself (inner-sphere disorder) can account for a portion of the observed $|\Delta\vec{\mu}|$ but that other symmetry breaking mechanisms, such as the outer-sphere disorder considered later, are needed to account for the remainder of the values observed experimentally.

Effect of Outer-Sphere Disorder (Disordered Solvent Environment) on Electronic Properties. The effects of outer-sphere disorder were investigated in two ways, first by surrounding a planar PPV-8 with explicit MeTHF molecules in a disordered arrangement to simulate the glassy environment and second by simulating the presence of a disordered solvent with a random dipole field (see Experimental Methods).

In the explicit MeTHF environments, the gas-phase $|\Delta\vec{\mu}|$'s obtained are similar to those obtained without the random environment (less than 1 D). However, when dielectric solvation

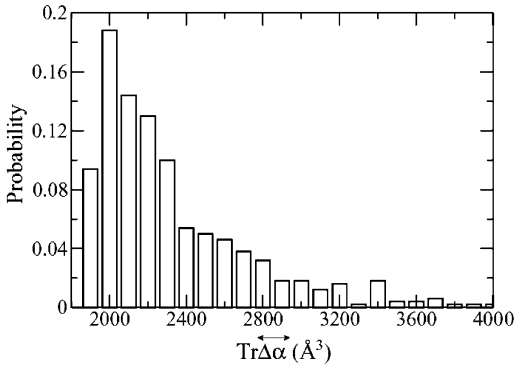

Figure 7. The distribution of tr $\overleftrightarrow{\Delta\alpha}$ for a planar PPV-8 surrounded by 500 different random dipole lattices. The lattice parameters are given in the Experimental Methods.

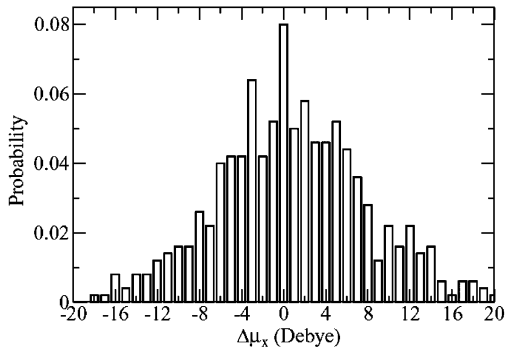

Figure 8. The distribution of $\Delta\mu_x$ for a planar PPV-8 surrounded by 500 different random dipole lattices. The lattice parameters are given in the Experimental Methods.

is included, values of $|\Delta\vec{\mu}|$ anywhere between 0 and 9 D are observed, depending on the specific MeTHF matrix used.

Although the large $|\Delta\vec{\mu}|$ values obtained for certain MeTHF matrixes are suggestive of the substantial values that can be induced by environmental asymmetry, it is more informative to obtain a statistical distribution of $\Delta\vec{\mu}$ over many random environments. To construct a more controlled and reproducible ensemble of environments, the lattice model of random dipoles described earlier was used. Because the Stark experiments measure the square of the dipole moment averaged over randomly oriented molecules within a solid sample, we will compare the experimental value to the root-mean-square of $\Delta\vec{\mu}$, rms-$\Delta\vec{\mu}$, obtained from 500 randomly generated lattices.

Figures 7 and 8, respectively, contain the distributions of tr $\overleftrightarrow{\Delta\alpha}$ and $\Delta\mu_x$ obtained from the dipole lattice model with lattice parameters chosen to mimic the overall dipole of the MeTHF solvent molecules (see Experimental Methods). Only $\Delta\mu_x$ is reported because, in all cases, the dipole moments are very small in both the *Y* and *Z* directions. These dipole lattices produce a rms-$\Delta\vec{\mu}$ of 7.5 D in a nominally symmetric oligomer, illustrating the large effects that the properties of the matrix can have on the electrooptical parameters. Consistent with what was seen earlier in the uniform dielectric model, the average values and the standard deviations of the $1B_u-mA_g$ energy gap and tr $\overleftrightarrow{\Delta\alpha}$ are, respectively, 0.65 ± 0.07 eV and 2300 ± 500 Å^3 (the median is ∼2200 Å^3 and the mode is ∼2000 Å^3). To summarize, the tr $\overleftrightarrow{\Delta\alpha}$ and the rms-$\Delta\vec{\mu}$ values are all in very good agreement with the Stark measurements reported here, and the $1B_u-mA_g$ energy difference is also within the range of 0.55−0.65 eV reported previously in the literature.[40,41]

Similar values to these are obtained for lattice parameters that are chosen to model CH bond dipoles (see Experimental Methods). This lattice leads to a rms-$\Delta\vec{\mu}$ of 8.4 D, a $1B_u-mA_g$ energy gap of 0.64 ± 0.08 eV, and a tr $\overleftrightarrow{\Delta\alpha}$ of 2400 ± 500 Å^3 (with median of ∼2200 Å^3 and mode of ∼2000 Å^3).

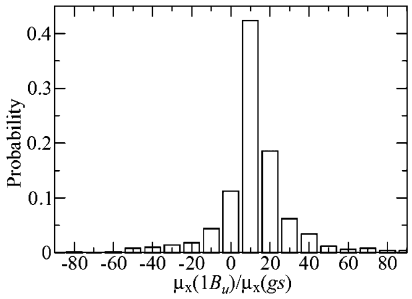

Figure 9. The distribution of $\mu_x(1B_u)/\mu_x(gs)$ for a planar PPV-8 surrounded by 500 random dipole lattices. The lattice parameters are given in the Experimental Methods.

The preceding results were obtained with the inclusion of dielectric screening. Without screening, the rms-$\Delta\vec{\mu}$ is only 1.7 D. This is similar to what was seen earlier for calculations using explicit MeTHF matrixes. The rms-$\Delta\vec{\mu}$ reflects the ability of the charges on the solvent to induce a dipole moment and is therefore related to the polarizability of the $1B_u$ state. Because inclusion of dielectric screening is required to reproduce the observed tr $\overleftrightarrow{\Delta\alpha}$, it is not surprising that dielectric screening must be included to obtain reasonable results for $\Delta\vec{\mu}$. In other words, *it is only when both solvation and the random charge environment are included that the experimental electrooptical properties can be reproduced.*

We note, however, that $\Delta\vec{\mu}$ is not simply related to tr $\overleftrightarrow{\Delta\alpha}$. That is, if the solvent could be viewed simply as applying a uniform static electric field to the oligomer, one would expect that the ratio $\mu_x(1B_u)/\mu_x(gs)$ would be given simply by the ratio of the polarizabilities of these two states because the polarizabilities are not strongly dependent on the strength of the local fields in the environment (i.e., the hyperpolarizabilities are small). Figure 9 shows that this is *not* the case, indicating that the electrostatic environment arising from permanent charges in the surroundings cannot be modeled by a simple uniform electric field. This is consistent with Kohler's finding that the electric field arising from the CH bond dipoles in an *n*-alkane matrix is very nonuniform.[29,30]

Summary and Conclusions

This paper presents experimental measurements of the change in polarizability (tr $\overleftrightarrow{\Delta\alpha}$) and permanent dipole moment ($|\Delta\vec{\mu}|$) accompanying photoexcitation from the ground electronic state to the $1B_u$ excited state of MEH−PPV polymer and several model oligomers in solvent glass matrixes. Computational studies of these properties, via INDO with single-configuration interaction (SCI) theory, reveal two roles played by the glassy environment.

The first role of the environment arises from the fast (optical) dielectric response of the medium, which screens the Coulomb interaction between the electron and hole present in the excited electronic states. This screening lowers the energy gap between the $1B_u$ and mA_g electronic states and increases the polarizability of the $1B_u$ state. A simple three-state model ($1A_g$, $1B_u$, and mA_g states) in which the oscillator strength between the $1B_u$ and mA_g is assumed to be independent of screening reproduces the results of the INDO/SCI calculations. Within this three-state model, the tr $\overleftrightarrow{\Delta\alpha}$ is a sensitive function of the energy gap between the $1B_u$ and mA_g electronic states, and the observed tr $\overleftrightarrow{\Delta\alpha}$, coupled with INDO/SCI's value for the oscillator strength

between the $1B_u$ and mA_g states, places this gap at 0.6 ± 0.05 eV. This is the most precise estimate of this energy gap available, although the accuracy of this estimate depends on the validity of INDO/SCI oscillator strength.

The second role played by the glassy environment is to break the symmetry of the nominally C_{2h} structure of the oligomer and polymer. This symmetry breaking gives rise to rather substantial experimentally observed $|\Delta\vec{\mu}|$'s of 6−11 D. The INDO/SCI calculations indicate that disorder in the ground-state geometry of the polymer (inner-sphere disorder) can account for roughly half of the observed $|\Delta\vec{\mu}|$. Disorder in the glassy environment (outer-sphere disorder) leads to a nonuniform electrostatic environment, and calculations indicate that this is also a substantial contributor to the observed $|\Delta\vec{\mu}|$. Note that substantial $|\Delta\vec{\mu}|$'s are observed only when the electron−hole screening effects arising from the fast dielectric response of the environment are taken into account. This screening weakens the attraction between the electron and hole such that disorder leads to more asymmetric distributions of the electron and hole and thereby larger observed dipole moments. Because $|\Delta\vec{\mu}|$ is zero in the absence of symmetry breaking, electroabsorption measurements provide a sensitive probe of the degree of disorder in these samples that may find applications, for instance, in screening materials. We are currently working on more detailed models of the interplay between inner-sphere and outer-sphere disorder that can serve as structure−property relations for interpreting the observed $|\Delta\vec{\mu}|$'s.

Acknowledgment. L.A.P. acknowledges NSF Grant CHE-0109761 and the Center for Molecular Analysis at CMU for use of the absorption spectrometer. D.J.Y. acknowledges NSF Grant CHE-9985719. In addition, we thank Dr. Chris Bardeen and Tom Bjorklund for the synthesis of the samples of PPV-3 and PPV-5 used in these experiments, Danny Lam for assisting in the initial phases of the computational work, and Dr. John Warman for helpful discussions.

Supporting Information Available: Details of the finite field calculations, further discussion of the use of Green's function, comparison of results for OPPV-9 and PPV-8, and details of modeling of outer-sphere disorder. This material is available free of charge via the Internet at http://pubs.acs.org.

References and Notes

(1) Burroughs, J. H.; Bradley, D. D. C.; Brown, A. R.; Marks, R. N.; Mackay, K.; Friend, R. H.; Burns, P. L.; Holmes, A. B. *Nature* **1990**, *347*, 539−541.

(2) Gustafsson, G.; Cao, Y.; Treacy, G. M.; Klavetter, F.; Colaneri, N.; Heeger, A. J. *Nature* **1992**, *357*, 477−479.

(3) Tessler, N.; Denton, G. J.; Friend, R. H. *Nature* **1996**, *382*, 695−697.

(4) Hide, F.; Schwartz, B. J.; Diaz-Garcia, M.; Heeger, A. J. *Chem. Phys. Lett.* **1996**, *256*, 424−430.

(5) Turnbull, G. A.; Andrew, P.; Jory, M. J.; Barnes, W. L.; Samuel, I. D. W. *Phys. Rev. B* **2001**, *64*, 125122/1−123122/6.

(6) Hoerhold, H.-H.; Tillmann, H.; Bader, C.; Klemm, E.; Holzer, W.; Penzkofer, A. *Proc. SPIE* **2002**, *4464*, 317−328.

(7) Chen, L.; McBranch, D. W.; Wang, H.-L.; Helgeson, R.; Wudl, F.; Whitten, D. G. *Proc. Natl. Acad. Sci.* **1999**, *96*, 12287−12292.

(8) Cornil, J.; dos Santos, D. A.; Crispin, X.; Silbey, R.; Bredas, J. L. *J. Am. Chem. Soc.* **1998**, *120*, 1289−1299.

(9) Nguyen, T.-Q.; Doan, V.; Schwartz, B. J. *J. Chem. Phys.* **1999**, *110*, 4068−4078.

(10) Nguyen, T.-Q.; Kwong, R. C.; Thompson, M. E.; Schwartz, B. J. *Appl. Phys. Lett.* **2000**, *76*, 2454−2456.

(11) Hu, D.; Yu, J.; Wong, K.; Bagchi, B.; Rossky, P. J.; Barbara, P. F. *Nature* **2000**, *405*, 1030−1033.

(12) Huser, T.; Yan, M.; Rothberg, L. J. *Proc. Natl. Acad. Sci.* **2000**, *97*, 11187−11191.

(13) Cadby, A. J.; Lane, P. A.; Mellor, H.; Martin, S. J.; Grell, M.; Giebeler, C.; Bradley, D. D. C.; Wohlgenannt, M.; An, C.; Vardeny, Z. V. *Phys. Rev. B* **2000**, *62*, 15604−15609.

(14) Collison, C. J.; Rothberg, L. J.; Treemaneekarn, V.; Li, Y. *Macromolecules* **2001**, *34*, 2346−2352.

(15) Korovyanko, O. J.; Vardeny, Z. V. *Chem. Phys. Lett.* **2002**, *356*, 361−367.

(16) Im, C.; Luptonl, J. M.; Schouwink, P.; Heun, S.; Becker, H.; Bassler, H. *J. Chem. Phys.* **2002**, *117*, 1395−1402.

(17) Horváth, Á.; Bässler, H.; Weiser, G. *Phys. Status Solidi B* **1992**, *173*, 755−764.

(18) Gelinck, G. H.; Piet, J. J.; Wegewijs, B. R.; Mullen, K.; Wildeman, J.; Hadziioannou, G.; Warman, J. M. *Phys. Rev. B* **2000**, *62*, 1489−1491.

(19) Premvardhan, L. L.; Wachsmann-Hogiu, S.; Peteanu, L. A.; Yaron, D. J.; Wang, P. C.; MacDiarmid, A. G. *J. Chem. Phys.* **2001**, *115*, 4359−4366.

(20) Moore, E. E.; Yaron, D. *J. Chem. Phys.* **1998**, *109*, 6147−6156.

(21) Mazumdar, S.; Guo, F. *J. Chem. Phys.* **1994**, *100*, 1665−1672.

(22) Gottfried, D. S.; Steffen, M. A.; Boxer, S. G. *Biochim. Biophys. Acta* **1991**, *1059*, 76−90.

(23) Gottfried, D. S.; Steffen, M. A.; Boxer, S. G. *Science* **1991**, *251*, 662−665.

(24) Ponder, M.; Mathies, R. *J. Phys. Chem.* **1983**, *87*, 5090−5098.

(25) Liptay, W.; Wortmann, R.; Bohm, R.; Detzer, N. *Chem. Phys.* **1988**, *120*, 439−448.

(26) Krawczyk, S.; Daniluk, A. *Chem. Phys. Lett.* **1995**, *236*, 431.

(27) Krawczyk, S.; Olszowka, D. *Chem. Phys.* **2001**, *265*, 335−347.

(28) Horváth, Á.; Weiser, G.; Baker, G. L.; Etemad, S. *Phys. Rev. B* **1995**, *51*, 2751−2758.

(29) Gradl, G.; Kohler, B. E.; Westerfield, C. *J. Chem. Phys.* **1992**, *97*, 6064−6071.

(30) Kohler, B. E.; Woehl, J. C. *J. Chem. Phys.* **1995**, *102*, 7773−7781.

(31) Locknar, S. A.; Chowdhury, A.; Peteanu, L. A. *J. Phys. Chem. B* **2000**, *104*, 5816−5824.

(32) Liptay, W. Dipole Moments and Polarizabilities of Molecules in Excited Electronic States. In *Excited States*; Lim, E. C., Ed.; Academic Press: New York, 1974; pp 129−229.

(33) Bublitz, G. U.; Boxer, S. G. *Annu. Rev. Phys. Chem.* **1997**, *48*, 213−242.

(34) Chowdhury, A.; Locknar, S. A.; Premvardhan, L. L.; Peteanu, L. A. *J. Phys. Chem. A* **1999**, *103*, 9614−9625.

(35) Premvardhan, L. L.; Peteanu, L. A. *J. Phys. Chem. A* **1999**, *103*, 7506−7514.

(36) Dewar, M. J. S.; Zoebisch, E. G.; Healy, E. F.; Stewart, J. J. P. *J. Am. Chem. Soc.* **1985**, *107*, 3902−3909.

(37) Tomlinson, A.; Yaron, D. J., manuscript in preparation.

(38) Kurtz, H. A.; Stewart, J. J. P.; Dieter, K. M. *J. Comput. Chem.* **1990**, *11*, 82−87.

(39) Pasquinelli, M. A. An Effective Particle Approach to the Photophysics of Conjugated Polymers. Ph.D. Thesis, Department of Chemistry, Carnegie Mellon University, Pittsburgh, PA, 2002.

(40) Leng, J. M.; Jeglinski, S.; Wei, X.; Benner, R. E.; Vardeny, Z. V.; Guo, F.; Mazumdar, S. *Phys. Rev. Lett.* **1994**, *72*, 156−159.

(41) Liess, M.; Jeglinski, S.; Vardeny, Z. V.; Ozaki, M.; Yoshino, K.; Ding, Y.; Barton, T. *Phys. Rev. B* **1997**, *56*, 15712−15724.

(42) Cornil, J.; Beljonne, D.; Heller, C. M.; Campbell, I. H.; Laurich, B. K.; Smith, D. L.; Bradley, D. D. C.; Mullen, K.; Brédas, J.-L. *Chem. Phys. Lett.* **1997**, *278*, 139−145.

(43) Bongiovanni, G.; Botta, C.; Brédas, J. L.; Cornil, J.; Ferro, D. R.; Mura, A.; Piaggi, A.; Tubino, R. *Chem. Phys. Lett.* **1997**, *278*, 146−153.

(44) Bjorklund, T.; Lim, S.-H.; Bardeen, C. J. *J. Phys. Chem. A* **2001**, *105*, 11970−11977.

(45) Gierschner, J.; Mack, H.-G.; Luer, L.; Oelkrug, D. *J. Chem. Phys.* **2002**, *116*, 8596−8609.

(46) Yu, J.; Hu, D.; Barbara, P. F. *Science* **2000**, *289*, 1327−1330.

(47) Warman, J. M.; Gelinck, G. H.; Piet, J. J.; Suykerbuyk, W. A.; de Haas, M. P.; Langeveld-Voss, B. M. W.; Janssen, R. A. J.; Hwang, D.-H.; Holmes, A. B.; Remmers, M.; Neher, D.; Mullen, K.; Bauerle, P. *Proc. SPIE* **1997**, *3145*, 142−149.

(48) Martin, S. J.; Bradley, D. D. C.; Lane, P. A.; Mellor, H.; Burn, P. L. *Phys. Rev. B* **1999**, *59*, 15133−15142.

(49) Rohlfing, F.; Bradley, D. D. C. *Chem. Phys.* **1998**, *227*, 133−151.

(50) Frese, R.; Oberheide, U.; van Stokkum, I.; van Grondelle, R.; Oelze, J.; van Amerongen, H. *Photosynth. Res.* **1997**, *54*, 115−126.

(51) Martin, S. J.; Mellor, H.; Bradley, D. D. C.; Burn, P. L. *Opt. Mater.* **1998**, *9*, 88−93.

(52) Tian, B.; Zerbi, G.; Schenk, R.; Mullen, K. *J. Chem. Phys.* **1991**, *95*, 3191−3197.

(53) Graham, S. C.; Bradley, D. D. C.; Friend, R. H.; Spangler, C. *Synth. Met.* **1991**, *41*, 1277.

(54) Meier, H.; Stalmach, U.; Kolshorn, H. *Acta Polym.* **1997**, *48*, 379.

(55) Hsu, J.-H.; Hayashi, M.; Lin, S.-H.; Fann, W.; Rothberg, L. J.; Perng, G.-Y.; Chen, S.-A. *J. Phys. Chem. B* **2002**, *106*, 8582−8586.

(56) van der Horst, J.-W.; Bobbert, P. A.; de Jong, P. H. L.; Michels, M. A. J.; Siebbeles, L. D. A.; Warman, J. M.; Gelink, G. H.; Brocks, G. *Chem. Phys. Lett.* **2001**, *334*, 303−308.